The Astrophysical Journal, 976:155 (14pp), 2024 December 1 https://doi.org/10.3847/1538-4357/ad86bc

Could the Interband Lag of Active Galactic Nucleus Vary Randomly?

Zhen-Bo Su[1,2], Zhen-Yi Cai[1,2], Jun-Xian Wang[1,2], Tinggui Wang[1,2], Yongquan Xue[1,2], Min-Xuan Cai[1,2], Lulu Fan[1,2,3], Hengxiao Guo[4], Zhicheng He[1,2], Zizhao He[5], Xu-Fan Hu[6], Ji-an Jiang[1,2], Ning Jiang[1,2], Wen-Yong Kang[1,2], Lei Lei[2,5], Guilin Liu[1,2], Teng Liu[1,2], Zhengyan Liu[1,2], Zhenfeng Sheng[3], Mouyuan Sun[7], and Wen Zhao[1,2]

[1] Department of Astronomy, University of Science and Technology of China, Hefei 230026, People's Republic of China; zbsu@mail.ustc.edu.cn, zcai@ustc.edu.cn
[2] School of Astronomy and Space Science, University of Science and Technology of China, Hefei 230026, People's Republic of China
[3] Deep Space Exploration Laboratory, Hefei 230088, People's Republic of China
[4] Shanghai Astronomical Observatory, Chinese Academy of Sciences, 80 Nandan Road, Shanghai 200030, People's Republic of China
[5] Purple Mountain Observatory, Chinese Academy of Sciences, Nanjing 210023, People's Republic of China
[6] Tsung-Dao Lee Institute, Shanghai Jiao-Tong University, Shanghai, 520 Shengrong Road, 201210, People's Republic of China
[7] Department of Astronomy, Xiamen University, Xiamen 361005, People's Republic of China
Received 2024 June 1; revised 2024 September 24; accepted 2024 October 13; published 2024 November 20

Abstract

The interband lags among the optical broad-band continua of active galactic nuclei (AGNs) have been intensively explored over the past decade. However, the nature of the lags remains under debate. Here, utilizing two distinct scenarios for AGN variability, i.e., the thermal fluctuation of accretion disk and the reprocessing of both the accretion disk and clouds in the broad line region, we show that, owing to the random nature of AGN variability, the interband lags of an individual AGN would vary from one campaign with a finite baseline to another. Specifically, the thermal fluctuation scenario implies larger variations in the lags than the reprocessing scenario. Moreover, the former predicts a positive correlation between the lag and variation amplitude, while the latter does not result in such a correlation. For both scenarios, averaging the lags of an individual AGN measured with repeated and nonoverlapping campaigns would give rise to a stable lag, which is larger for a longer baseline and gets to saturation for a sufficiently long baseline. However, obtaining the stable lag for an individual AGN is very time-consuming. Alternatively, it can be equivalently inferred by averaging the lags of a sample of AGNs with similar physical properties, and thus can be properly compared with predictions of AGN models. In addition, several new observational tests suggested by our simulations are discussed, as well as the role of the deep high-cadence surveys of the Wide Field Survey Telescope in enriching our knowledge of the lags.

Unified Astronomy Thesaurus concepts: Time domain astronomy (2109); Active galactic nuclei (16)

1. Introduction

Active galactic nuclei (AGNs) have long been postulated to be powered by the process of gas accretion into a supermassive black hole (BH), resulting in the formation of an accretion disk and producing enormous energy radiations over the whole electromagnetic spectrum. Hitherto, the most widely adopted model for the accretion disk in AGNs has been the optically thick and geometrically thin disk model (N. I. Shakura & R. A. Sunyaev 1973; hereafter the SSD model), though its validation has long been questioned (e.g., R. Antonucci 2013, 2015, 2018; R. R. J. Antonucci 2023; Z.-Y. Cai & J.-X. Wang 2023).

Notwithstanding the fact that the accretion disks in almost all AGNs are currently inaccessible to direct imaging, two alternative methods have been proposed to infer the disk size. One probe is microlensing, by which the emission from a smaller disk region of a background quasar (i.e., the very luminous AGN) could be more significantly fluctuated by stars in the foreground lensing galaxy. Up to now, the microlensing probe has been utilized in only tens of gravitationally lensed quasars (e.g., J. Jiménez-Vicente et al. 2014; N. F. Bate et al. 2018; M. A. Cornachione & C. W. Morgan 2020) and the inferred disk sizes in optical are generally found to be larger than the SSD prediction by ∼0.5 dex on average (e.g., X. Dai et al. 2010; C. W. Morgan et al. 2018).

Another probe is the so-called continuum reverberation mapping (CRM), in which the UV/optical continuum variation is assumed to be driven by heating of the fluctuating X-ray emission from the vicinity of the central BH, so the variation at shorter wavelength from the inner disk leads that at longer wavelength from the outer disk (J. H. Krolik et al. 1991). This assumption is usually designated as X-ray reprocessing. Compared to the microlensing method, the CRM method is more attractive because it can be applied to a large number of nonlensed normal AGNs and quasars whose multiband light curves (LCs) are easily obtained in the time domain era. Now, disk sizes of several hundreds of normal AGNs and quasars have been estimated using the CRM method, and hundreds of thousands more would be available thanks to several ongoing and upcoming high-cadence multiwavelength surveys (e.g., W. N. Brandt et al. 2018; T. Wang et al. 2023).

A small number of AGNs and quasars have been well monitored in multiple UV/optical bands, either in daily cadence within one year, e.g., the AGN Space Telescope and Optical Reverberation Mapping project (STORM; G. De Rosa et al. 2015) and alike successors, or in sparser cadence ($\gtrsim$3–7 days) but over several years, e.g., the Zwicky Transient Facility survey (ZTF; M. J. Graham et al. 2019), the Pan-STARRS1 survey (PS1; K. C. Chambers et al. 2016), the Sloan Digital Sky Survey Reverberation Mapping project (SDSS-RM; Y. Shen et al. 2015), and the Dark Energy Survey

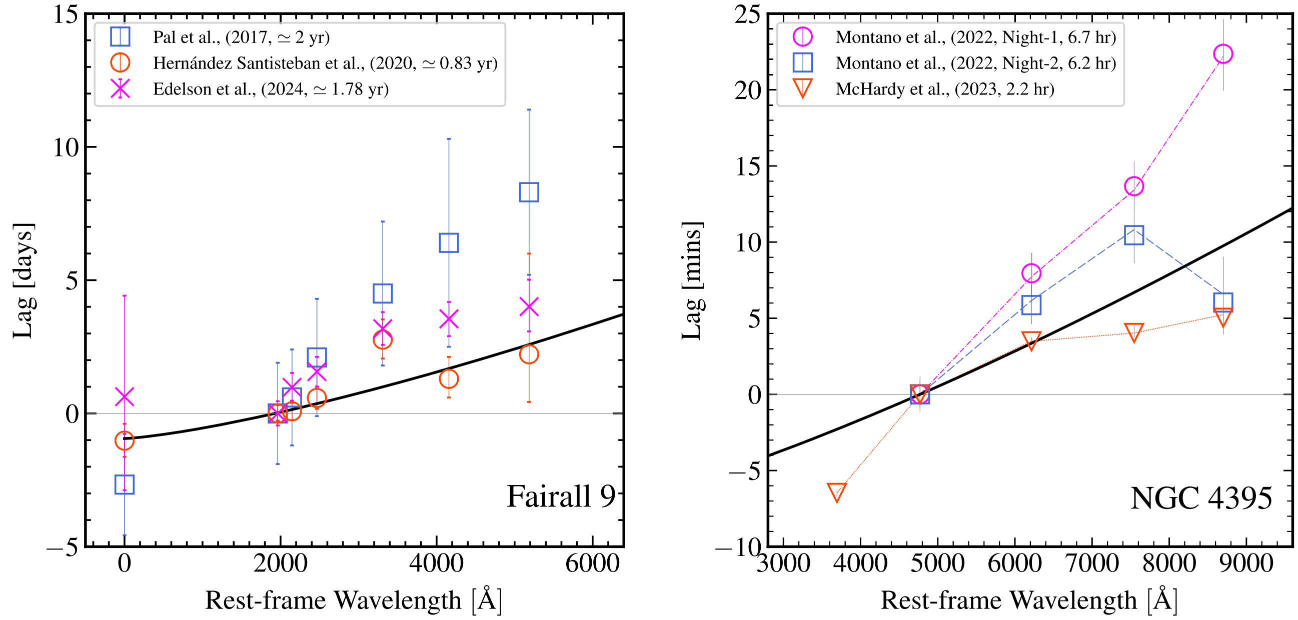

Figure 1. The potentially varied lag-wavelength relations observed in two AGNs. Left-hand panel: Relative to the Swift-UVW2 band at 2055 Å, the lag-wavelength relations for Fairall 9 are measured in three distinct periods by M. Pal et al. (2017, from 2013 April to 2015 April), J. V. Hernández Santisteban et al. (2020, from 2018 May to 2019 February) and R. Edelson et al. (2024, from 2018 May to 2020 February). Only the Swift bands are shown as R. Edelson et al. (2024). The black solid line indicates the SSD-predicted lag-wavelength relation for Fairall 9 using a BH mass of $2.6 \times 10^8 M_{\odot}$ and an Eddington ratio of 0.02 (R. V. Vasudevan & A. C. Fabian 2009). Right-hand panel: Relative to the g band, the lag-wavelength relations for NGC 4395 are measured in three nights by I. M. McHardy et al. (2023, 2.2 hr in 2018 April) and J. W. Montano et al. (2022, 6.7 and 6.2 hr in 2022 April 26 and 27, respectively). The black solid line is the SSD-predicted lag-wavelength relation implied by a BH mass of $1.7 \times 10^4\ M_{\odot}$ (H. Cho et al. 2021) and a bolometric luminosity of 5.3×10^{40} erg s^{-1} (E. C. Moran et al. 2005). Here, the SSD-predicted lag-wavelength relations are simply given by Equation (12) of M. M. Fausnaugh et al. (2016) assuming $\eta = 0.1$, $\kappa = 1$, and $X = 5.04$ (S. S. Tie & C. S. Kochanek 2018).

(DES; T. M. C. Abbott et al. 2018). However, conflicting results have been obtained when applying the CRM method to these observations. The disk sizes of some AGNs and quasars are found to be larger than the SSD prediction by a factor of ∼2–10 (e.g., M. M. Fausnaugh et al. 2016; M. Pal et al. 2017; Y.-F. Jiang et al. 2017; E. M. Cackett et al. 2018; M. M. Fausnaugh et al. 2018; R. Edelson et al. 2019; H. Guo et al. 2022; W.-J. Guo et al. 2022; V. K. Jha et al. 2022; J. W. Montano et al. 2022; E. Kara et al. 2023), while some others are consistent with or just slightly larger than the SSD prediction (e.g., M. Kokubo 2018; D. Mudd et al. 2018; Y. Homayouni et al. 2019; J. V. Hernández Santisteban et al. 2020; Z. Yu et al. 2020; V. K. Jha et al. 2022). Meanwhile, the disk size discrepancy appears less prominent for more luminous (T. Li et al. 2021) and massive (H. Guo et al. 2022) AGNs.

The origin of the disk size discrepancy between observed and SSD-predicted is still unclear but many solutions to the discrepancy have been proposed, including the inhomogeneous disk fluctuation (J. Dexter & E. Agol 2011), the internal reddening of AGN host galaxy (C. M. Gaskell 2017), the departure from nonblackbody emission (P. B. Hall et al. 2018), the role of disk wind (Y.-P. Li et al. 2019; M. Sun et al. 2019), and the diffuse continuum emission (DCE) from the broad-line region (BLR; E. M. Cackett et al. 2018; D. Chelouche et al. 2019; H. Netzer 2022; J. W. Montano et al. 2022). All of them are based on the reprocessing scenario and the origin of the interband lag is the differential light traveling. Actually, a new origin for the interband lag as a result of the differential regression capability of local thermal fluctuation (or the differential capability of re-establishment of local thermal equilibrium after being perturbed) has been proposed (Z.-Y. Cai et al. 2018; Z.-Y. Cai et al. 2020; M. Sun et al. 2020). According to the thermal fluctuation scenario, the measured interband lags are no longer simply related to the light-traveling time, and thus the disk size. In other words, the origin of the lags should be clearly understood before utilizing the lag to estimate the disk size. Here, a relevant question to be resolved by upcoming surveys is whether the lags measured in different periods are stable.

Even good stability of the lags inferred from repeated multiyear campaigns has been reported for a few AGNs, e.g., Mrk 279 (D. Chelouche et al. 2019) and Mrk 110 (F. M. Vincentelli et al. 2022), and it is highly intriguing that potentially varied lags have been unveiled in some AGNs. First, in a radio-quiet Seyfert type 1 AGN, Fairall 9 (the left-hand panel of Figure 1), M. Pal et al. (2017) found very large lags, inconsistent with the SSD prediction, using observations from 2013 April to 2015 April, while J. V. Hernández Santisteban et al. (2020) showed small lags utilizing observations from 2018 May to 2019 February. Further extending the baseline (from 2018 May to 2020 February) for Fairall 9, R. Edelson et al. (2024) recently reported lags larger[8] than J. V. Hernández Santisteban et al. (2020), albeit with substantial errors. Second, a similar result has been unveiled in the dwarf Seyfert 1 galaxy NGC 4395 (the right-hand panel of Figure 1). Although the lags of the r (i or z) band relative to the g band between two successive nights of J. W. Montano et al. (2022, on 2022 April 26 and 27) differ somewhat at $\simeq 1.1\sigma$ ($\simeq 1.3\sigma$ or $\simeq 4.5\sigma$) confidence level, the differences[9] become very significant at

[8] However, R. Edelson et al. (2024) suggested the lags are quite stable among four periods of ∼160 days.

[9] The differences in the mean flux densities between I. M. McHardy et al. (2023) and J. W. Montano et al. (2022) are smaller than 17% and thus cannot be responsible for the lag difference.

$\simeq 3.2\sigma$ ($\simeq 5.8\sigma$ or $\simeq 7.0\sigma$) confidence level once comparing the lags measured by J. W. Montano et al. (2022, the first night) and by I. M. McHardy et al. (2023, 2018 April 16). Third, F. M. Vincentelli et al. (2023, see their Figure 3) reported a significant lag change between two ~two-month periods for NGC 7469.

Although the change of the lags could be attributed to distinct observational conditions met by various studies (e.g., different photometric uncertainty and sampling cadence), finite realizations of a stochastic process (W. F. Welsh 1999), unresolved problems in data reduction (I. M. McHardy et al. 2023), or improper methodologies adopted (J. H. H. Chan et al. 2020), does the aforementioned potential change of the lags in a few AGNs hint at a random nature for the lags among UV/optical continua? Actually, the lag randomness has been predicted by the thermal fluctuation scenario (Z.-Y. Cai et al. 2018; Z.-Y. Cai et al. 2020; M. Sun et al. 2020), while the conventional reprocessing over an SSD disk gives rise to quite stable lags (M. Sun et al. 2019; F. M. Vincentelli et al. 2022). Note that a larger scatter in the lags predicted by the reprocessing scenario is possible once considering either a dynamical driving source, e.g., the dynamical evolution of the corona height (E. S. Kammoun et al. 2021), or a variable contribution of the BLR emission (V. K. Jaiswal et al. 2023; F. M. Vincentelli et al. 2023).

In this work, being different from the general simulations in the framework of reprocessing (e.g., J. H. H. Chan et al. 2020; Z. Yu et al. 2020; A. B. Kovačević et al. 2021, 2022; F. Pozo Nuñez et al. 2023) for the Deep Drilling Fields (DDFs) of the Vera C. Rubin Observatory Legacy Survey of Space and Time (LSST; W. N. Brandt et al. 2018), we also utilize the up-to-date thermal fluctuation model (Section 2) to quantitatively predict the lag randomness using simulations for AGNs in analog to the famous Seyfert 1 galaxy NGC 5548, and present distinguishable properties on the lags predicted by the two distinct scenarios for AGN variability (Section 3). Next, in Section 4 we anticipate how surveys to be conducted by the 2.5-meter Wide Field Survey Telescope (WFST equipped with five SDSS-like *ugriz* filters; T. Wang et al. 2023) can help improve our understanding on the multiwavelength AGN variability and the associated interband lags. Finally, our brief conclusions are presented in Section 5.

2. Models for the Optical Variability of AGN

Several models have been proposed to account for the optical multiband variation properties of AGNs, such as NGC 5548 in particular, which has been intensively monitored for half a year from 2014 January to July (M. M. Fausnaugh et al. 2016). In other words, models are generally constrained by such observations with limited lengths. However, the constrained models are helpful in not only predicting the variation properties at timescales longer than observed but also providing a way of taking the effect of the randomness of AGN variability into account.

Here, we adopt two distinct models: the thermal fluctuation model (Section 2.1; Z.-Y. Cai et al. 2018, 2020) and the reprocessing model with DCE, including emissions from both the accretion disk and clouds in the BLR (Section 2.2; E. M. Cackett et al. 2022; V. K. Jaiswal et al. 2023). Utilizing 200 different realizations of 10 yr long WFST-*ugriz* LCs implied by both models, we will show that the dispersions of the lag-wavelength relations predicted by them are very different, and thus can be used to distinguish models for AGN variability.

2.1. Thermal Fluctuation Model

Previously, Z.-Y. Cai et al. (2018, 2020) developed a thermal disk model, exploring the UV/optical continuum lag in AGNs (EUCLIA), in which the UV/optical/X-ray variations are all attributed to disk/corona turbulence, contrary to the reprocessing scenario where the UV/optical variations are due to the varying X-ray/EUV heating. Actually, there are some known challenges to the reprocessing scenario, including (1) there is a possible deficit of the X-ray energy budget (e.g., C. M. Gaskell et al. 2007); (2) sometimes poor coordination is observed between X-ray and UV/optical variations (D. Maoz et al. 2002; C. M. Gaskell 2006; D. Starkey et al. 2017; L. C. Gallo et al. 2018; A. M. Morales et al. 2019; H. Sou et al. 2022); (3) too much high-frequency power is predicted (E. Gardner & C. Done 2017); (4) UV/optical variation amplitudes that are too small are predicted (H. Sou et al. 2022); (5) time lags that are too small are predicted (see references in Section 1); and (6) timescale dependence of the color variation that is too weak is predicted (F.-F. Zhu et al. 2018).

Serving as a choice to circumvent or overcome these challenges encountered by the reprocessing model, Z.-Y. Cai et al. (2018) propose that the interaction between the local temperature fluctuation and a common large-scale fluctuation can naturally generate the AGN lags across UV/optical to X-ray. A scene where both disk and corona are coupled through magnetic fields provides an attractive physical mechanism responsible for the common large-scale fluctuation (M. Sun et al. 2020).

This new scenario introduces a novel origin for the AGN interband lag as a result of the differential regression capability among distinct disk regions. When responding to a common large-scale fluctuation, the local fluctuation in the inner disk region generating emission at the shorter wavelength regresses more quickly, due to the shorter local damping timescale of the temperature fluctuation, than that in the outer disk region radiating at the longer wavelength. Therefore, the implied AGN continuum at the longer wavelength naturally lags that at the shorter wavelength, which is nicely consistent with the lag measurements on local Seyfert galaxies (Z.-Y. Cai et al. 2018, 2020). In addition, extending to X-ray, this framework also successfully accounts for the puzzling large UV to X-ray lags found in several local galaxies (Z.-Y. Cai et al. 2020).

As Z.-Y. Cai et al. (2020) have pointed out, the random turbulence in the EUCLIA model could naturally yield randomness in lag measurements, and even reverse lags, i.e., UV leading X-ray instead of X-ray leading UV, as found in Mrk 509 (R. Edelson et al. 2017, if dividing their LCs into two parts) and Mrk 335 (E. Kara et al. 2023, comparing observations on the high state in 2008 and the low state in 2020, see their Figure 7).

A comparison of the thermal fluctuation model EUCLIA quantitatively to all individual AGNs with available lag measurements will be detailed in a companion paper (Z. B. Su et al. 2024a, in preparation). In this work, we make a prediction on the randomness of the optical interband lags for AGNs with similar BH mass and Eddington ratio to NGC 5548 (hereafter, N5548-like AGNs; see Section 4.2 for details). NGC 5548 is a Seyfert 1 galaxy at $z = 0.01067$ with $M_{\rm BH} \simeq 5 \times 10^7 M_\odot$ and $\lambda_{\rm Edd} \simeq 0.05$ and has been largely used to calibrate our model.

See Z.-Y. Cai et al. (2018, 2020) for details and model parameters.

2.2. Reprocessing Model

The conventional interpretation of the interband lags among UV/optical LCs is that the variability of UV/optical emission originates from the accretion disk heated by a varying ionizing source above the central BH, and the lags correspond to the time difference of the reverberation signals reflected between different disk regions (E. M. Cackett et al. 2021). To overcome the too small lag predicted by the traditional reprocessing model, contamination from other more distant reprocessors, such as clouds in the BLR, has been proposed (E. M. Cackett et al. 2018; D. Chelouche et al. 2019; J. W. Montano et al. 2022; H. Netzer 2022; S. Hagen et al. 2024). In the following, we adopt the simplest reprocessing model with DCE[10] to simulate the optical LCs by convolving a driving LC with given response functions, which account for both the reverberation signal from disk and contributions of the DCE in different bands.

Suggested by E. Gardner & C. Done (2017) and following F.-F. Zhu et al. (2018), we assume that the driving LC is described by the damped random walk (DRW) model with parameters determined from modeling the observed Swift-UVW2 LC of NGC 5548. We adopted a damping timescale of 94.8 days and a mean flux of $2.527 \times 10^{-14}\,\mathrm{erg\,cm^{-2}\,s^{-1}\,\AA^{-1}}$ determined by F.-F. Zhu et al. (2018) using a $\sim$2 yr UVW2 LC, while a variability amplitude of $0.419 \times 10^{-14}\,\mathrm{erg\,cm^{-2}\,s^{-1}\,\AA^{-1}}$ (smaller by a factor of 1.77 than determined by F.-F. Zhu et al. 2018 but equivalent to the fractional variability of 0.166 determined by M. M. Fausnaugh et al. 2016) in order to match the observed *ugriz* variability amplitudes of NGC 5548 measured for the same $\sim$6 months monitoring (see Section 2.3).

Following E. M. Cackett et al. (2022) and V. K. Jaiswal et al. (2023), we assumed $\psi_{\rm total}(\tau|\lambda) = (1-f)\psi_{\rm disk}(\tau|\lambda) + f\psi_{\rm BLR}(\tau)$ as the total response function accounting for the reverberation signals from both the disk,[11] $\psi_{\rm disk}$ (D. Starkey et al. 2017, see their Equations (19)–(23), and clouds in BLR, $\psi_{\rm BLR}$ (E. M. Cackett et al. 2022, see their Equation (5)), i.e., $\psi_{\rm BLR}(\tau|S, M) = 1/S\tau\sqrt{2\pi} \times \exp[-(\ln\tau - M)^2/2S^2]$, where $M \simeq \ln(7.3/\mathrm{days})$ and $S = 1.1$ are the best-fit values for NGC 5548 from E. M. Cackett et al. (2022). Values for the response fraction from the BLR, f, also come from fits to the lag-frequency spectra of NGC 5548 by (E. M. Cackett et al. 2022, their Figure 7).

In this work, we adopt a simplified approach to model the effect of the BLR continuum emission on the lags. Our analysis has not yet considered other known BLR-related phenomena, such as the "breathing" effect (E. M. Cackett & K. Horne 2006) and the "holiday" anomaly (M. R. Goad et al. 2016), which can also contribute to the scatter in the lags to be discussed in the following and should be incorporated into a more physical BLR model in the future.

2.3. Simulation Setting

For the aforementioned two scenarios for AGN variability, we simulate both ideal and mock LCs in the five WFST-*ugriz* bands for 200 N5548-like AGNs. The ideal LCs span 10 yr with a very fine sampling cadence of 0.1 day and without photometric uncertainty, while the mock LCs are obtained by sampling the ideal ones to which observational conditions are complemented as real as possible.

As a result of the season gap, some AGNs can only be continuously observed for a limited duration throughout the year (hereafter, the duration, $\mathcal{M}$, in units of month), though they can be repeatedly monitored for several years (hereafter, the baseline, $\mathcal{Y}$, in units of year). Furthermore, sparse (longer than $\sim$day) and irregular sampling cadences (hereafter, the cadence, $\mathcal{C}$, in units of day) are popular in the current time domain surveys for AGNs, whose photometry is affected by the measurement error (hereafter, the photometric uncertainty, $\sigma_{\rm e}$, in units of mag).

Thanks to the AGN STORM project (M. M. Fausnaugh et al. 2016), NGC 5548 was intensively monitored ($\mathcal{C} \simeq 1$) by ground-based telescopes in the SDSS-*ugriz* bands over $\simeq$6 months duration ($\mathcal{M} \simeq 6$) within one year ($\mathcal{Y} = 1$). According to the *ugriz* LCs of M. M. Fausnaugh et al. (2016), the *u*-, *g*-, *r*-, *i*-, and *z*-band median apparent magnitudes are $\simeq$13.98 mag, $\simeq$13.93 mag, $\simeq$13.13 mag, $\simeq$13.14 mag, and $\simeq$12.85 mag with median $\sigma_{\rm e}$ (including both measurement and calibration uncertainties in units of magnitude) of $\simeq$0.038 mag, $\simeq$0.036 mag, $\simeq$0.034 mag, $\simeq$0.023 mag, and $\simeq$0.013 mag, respectively. Following S. Vaughan et al. (2003, their Equation (8)), we find that for the duration of $\sim$6 months the observed variation amplitudes, $\sigma_{\rm rms}$, after removing the contamination from host galaxy for NGC 5548 are $\simeq$0.13 mag, $\simeq$0.10 mag, $\simeq$0.06 mag, $\simeq$0.08 mag, and $\simeq$0.05 mag for the *u*, *g*, *r*, *i*, and *z* bands, respectively.

For comparison, the means and standard deviations of our $\sigma_{\rm rms}$ simulated for the same duration of $\sim$6 months under the thermal fluctuation model are 0.11 ± 0.03 mag, 0.10 ± 0.03 mag, 0.08 ± 0.02 mag, 0.07 ± 0.02 mag, and 0.06 ± 0.02 mag for the *u*, *g*, *r*, *i*, and *z* bands, respectively. For the reprocessing model with DCE,[12] the resultant $\sim$6 months $\sigma_{\rm rms}$ is 0.10 ± 0.04 mag, which is nearly the same for all *ugriz* bands. Thus, for both scenarios, our simulations for N5548-like AGNs result in $\sigma_{\rm rms}$ comparable to those measured in $\sim$6 months for NGC 5548.

The variation significance, $\mathrm{SNR}_\sigma \equiv \sigma_{\rm rms}/\sigma_{\rm e}$, is a more important factor than $\sigma_{\rm e}$ in determining whether the interband lags can be successfully measured. We find that the observed SNR_σ for NGC 5548 are $\simeq$3.3, 2.6, 1.8, 3.0, and 3.4 for the *u*, *g*, *r*, *i*, and *z* bands, respectively. Therefore, we would conservatively adopt $\mathrm{SNR}_\sigma \simeq 3$ as a reference for all bands in our fiducial simulations and discuss how worse and better photometric uncertainties, i.e., $\mathrm{SNR}_\sigma \simeq 1$ and 9, would affect the results.

To mimic the real observations, we assume that when sampling an ideal LC the observed epochs are randomly located within four hours before and after midnight. In addition, for a given SNR_σ, magnitudes at all sampled epochs are fluctuated by random Gaussian deviates according to a

[10] Other reprocessing-related models, such as windy disk (M. Sun et al. 2019), rimmed/tilted accretion disk (D. A. Starkey et al. 2023), and inward disk propagation with reverberation from the disk and wind (S. Hagen et al. 2024), are worthy of further investigation.

[11] https://github.com/drds1/astropy_stark/blob/master/astropy_stark/mytfb_quick.py

[12] The variation amplitude predicted by the reprocessing model is generally rescaled to match the observed value. Although the rescaling does not affect measuring the lag, the wavelength dependence of the variation amplitude is an important property of AGN variability and should be self-consistently addressed by future sophisticated reprocessing models.

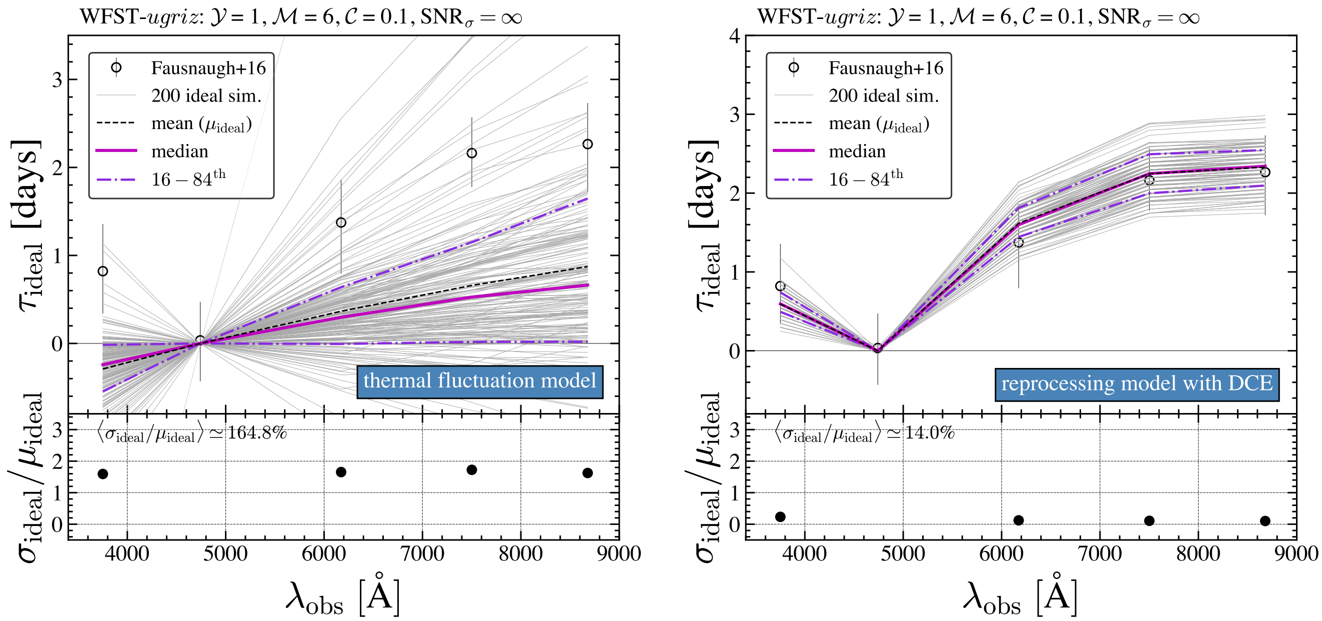

Figure 2. Left-hand panel: Relative to the WFST-g band, the lag-wavelength relations for N5548-like AGNs predicted by the thermal fluctuation scenario are compared to the measured one (open circles) adopting the ∼6 month *ugriz* LCs of NGC 5548 from M. M. Fausnaugh et al. (2016). The predicted lag-wavelength relations are derived from 200 independent ideal simulations (gray thin solid lines) for N5548-like AGNs monitored over 6 months duration ($\mathcal{M}=6$) within one year ($\mathcal{Y}=1$) and with a very fine cadence of 0.1 day ($\mathcal{C}=0.1$) in the five WFST-*ugriz* bands. Here, the ideal case is considered without photometric uncertainty ($\sigma_e=0$ or $\mathrm{SNR}_\sigma=\infty$). Accordingly, the median (thick solid line), mean (thin dashed line), and 16%–84% percentile ranges (thin dotted–dashed lines) of the 200 ideal lag-wavelength relations are shown. Although the 1σ dispersion of lags, $\sigma_{\rm ideal}$, is larger at longer wavelengths, similar relative scatters of lags are found for all bands as indicated by similar $\sigma_{\rm ideal}/\mu_{\rm ideal}$ (filled circles in the lower panel), where $\mu_{\rm ideal}$ is the corresponding mean lag. Right-hand panel: Same as the left-hand panel, but for the prediction of the reprocessing model with DCE. We note that the relative scatters of the lags predicted by the reprocessing model with DCE are smaller than the thermal fluctuation model.

specific photometric uncertainty of $\langle\sigma_{\rm rms}\rangle/\mathrm{SNR}_\sigma$, where $\langle\sigma_{\rm rms}\rangle$ is the mean of variation amplitudes of all simulated LCs for a given band.

3. The Interband Lag of AGN

3.1. Does the Interband Lag Vary?

Adopting $\mathcal{Y}=1$, $\mathcal{M}=6$, $\mathcal{C}=0.1$, and $\mathrm{SNR}_\sigma=\infty$ (i.e., $\sigma_e=0$), we first demonstrate that varied lags are predicted by both the thermal fluctuation model and the reprocessing model with DCE. The variation of the lags is intrinsically attributed to the random nature of AGN variability, although in reality both the sparse sampling and uncertainty of measurements would contribute to the variation to some extent. We adopt the physical parameters of NGC 5548, apply them to both AGN variability models, and perform 200 independent simulations to mimic WFST observations on 200 N5548-like AGNs. For the simulated WFST-*ugriz* LCs of every AGN, we use the standard interpolated cross-correlation function (CCF) technique[13] (e.g., B. M. Peterson et al. 1998; M. Sun et al. 2018) to measure the interband lags relative to the g band. We consider a broad enough range spanning −50 to 50 days to search the CCF for the centroid lag, τ, defined by CCF-weighted averaging the lags whose correlation coefficients, $r_{\rm cc}(\tau)$, are larger than 80% of the maximum. Then, there is a lag-wavelength relation for every N5548-like AGN. Note that, in addition to the CCF method adopted here, other methods, such as the frequency-resolved technique (A. Zoghbi et al. 2013; E. M. Cackett et al. 2022) and the wavelet transform method (D. R. Wilkins 2023), may be helpful in unveiling the nature of the AGN lags.

The lag-wavelength relations of 200 N5548-like AGNs predicted by the thermal fluctuation model and the reprocessing model with DCE are shown as gray solid lines in the left- and right-hand panels of Figure 2, respectively. The predicted lag-wavelength relations are intriguingly diverse for both models. It is easy to notice that both the lags and the lag scatters are statistically larger at longer wavelengths, but the relative scatter of the lags, defined as the ratio of the lag scatter to the mean lag, are nearly identical across wavelengths. Given $\mathcal{M}=6$ and $\mathcal{Y}=1$, the thermal fluctuation model implies a relative scatter in the lags of ∼165%, which is significantly larger than the ∼14% implied by the reprocessing model with DCE. For comparison, the reprocessing model without DCE (i.e., disk only) implies a relative scatter in the lags of only ∼7%. Note that the relative scatter of the lags decreases as the duration/baseline of the LC increases.

For the reprocessing models, the CCF between two bands is related to the auto-correlation function (ACF) of the driving LC and to the given transfer functions of the two bands. Since the ACF of the driving LC is determined by the power spectral density (e.g., R. A. Edelson & J. H. Krolik 1988; W. F. Welsh 1999), which changes from one finite duration to another owing to the random nature of AGN variability, the resultant is a scatter in the lag-wavelength relations. Furthermore, the reprocessing model with DCE, involving more distant reverberation signals from BLR and thus longer light-traveling times, results in a larger scatter in the lag-wavelength relations than the reprocessing model without DCE.

In contrast, the interband lags in the thermal fluctuation scenario are attributed to the differential regression capability of local fluctuations, which is likely related to the thermal timescales. Thus, the complicated origin of the lags in the

[13] PyCCF: https://www.ascl.net/1805.032.

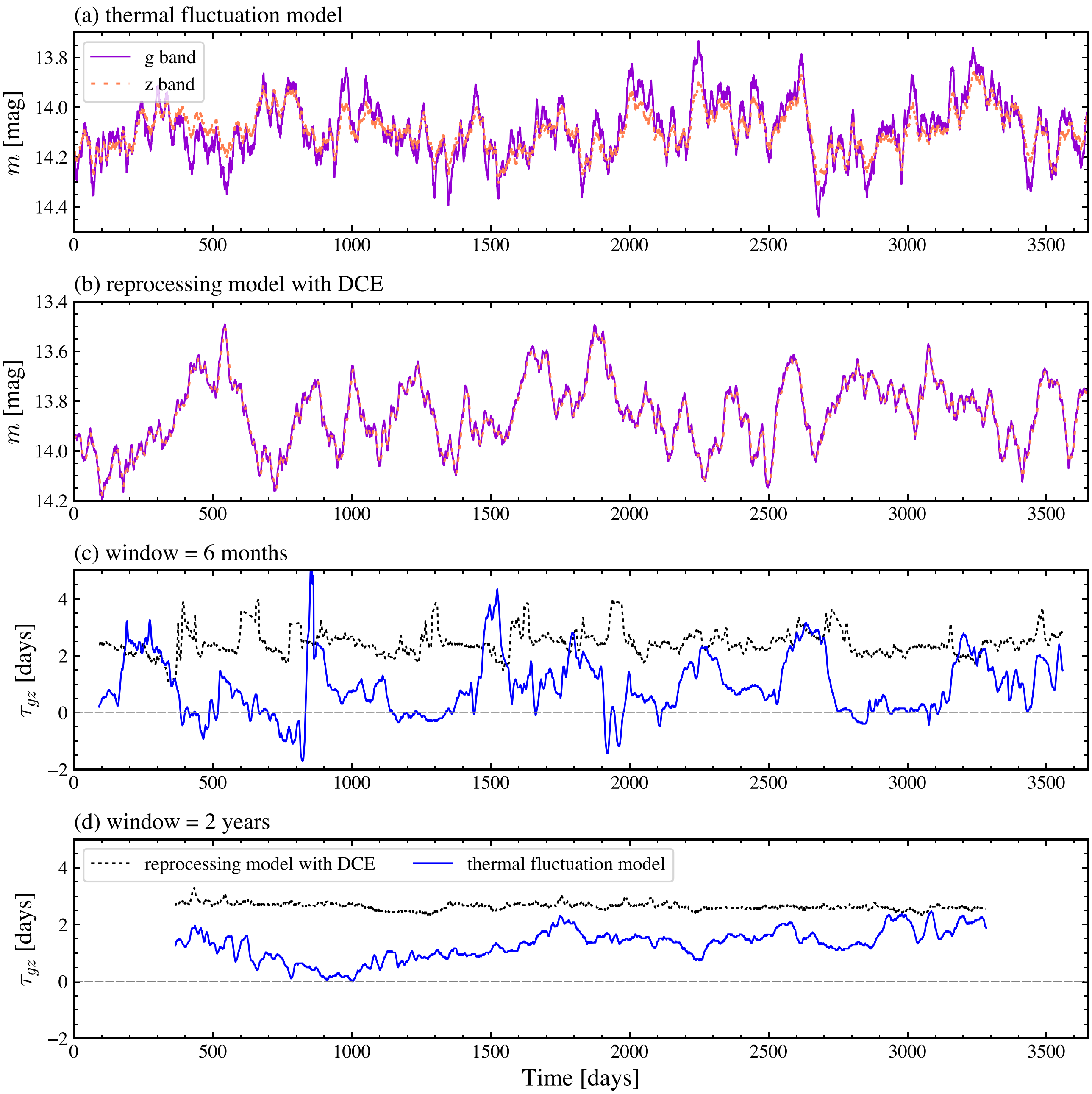

Figure 3. An illustration of the simulated 10 yr ideal LCs (g band vs. z band) for the thermal fluctuation model (panel a) and the reprocessing model with DCE (panel b). Using part of LCs blanketed by a moving window of 6 months (or 2 yr) to measure the interband lags between g and z bands, the evolution of τ_{gz} with time for both models are presented in panel (c) (or panel (d)). Being consistent with the results shown in Figure 2, the lag evolution implied by the thermal fluctuation model exhibits larger variation than the reprocessing model with DCE. As the size of the moving window increases, the lag evolution becomes less variable for both models.

thermal fluctuation model is expected to result in a larger scatter in the lag-wavelength relations than the reprocessing model with DCE.

The potential change of the lags observed in a few AGNs (see Introduction and Figure 1) may support our simulation results, but more observational tests are demanded. Using long-term photometric surveys such as ZTF, there are hints at the lag change for individual AGNs (Z. B. Su et al. 2024b, in preparation). It is interesting to note that a large scatter in the ratios of the measured lags to the SSD-predicted lags was reported in a sample of 95 quasars from the SDSS-RM project (e.g., Y. Homayouni et al. 2019; H. W. Sharp et al. 2024), which may also hint at lag randomness.

3.2. How Do the Interband Lags Evolve with Time?

In Figure 3, we present distinguishable predictions of both the thermal fluctuation model and reprocessing model with DCE on the lags evolution. We find that the correlation time for a significant lag change differs from the damping timescale (or auto-correlation timescale) of a single-band LC and depends on the duration of the LC used to measure the lags. A longer duration of the LC results in a smoother lag evolution, indicating a longer correlation time for the lag change. Thus, how the lags evolve with time and what is the relationship between the lag evolution behavior and the chosen duration/baseline of the LC are new questions to be addressed by future monitoring of AGNs.

3.3. Is there Always a u-band Excess?

In the 6 months campaign for NGC 5548 by M. M. Fausnaugh et al. (2016), there is a clear *u*-band excess in the lag-wavelength relation, i.e., the *u*-band variation delays rather than leads the *g*-band variation (Figure 2). The *u*-band excess has been observed in many AGNs and is widely thought to be the result of contamination from the diffuse BLR emission (e.g., E. M. Cackett et al. 2018; D. Lawther et al. 2018; D. Chelouche et al. 2019; K. T. Korista & M. R. Goad 2019; H. Guo et al. 2022; J. W. Montano et al. 2022; H. Netzer 2022). However, for several AGNs, repeated observations on Mrk 110 show that the *u*-band excess does not always exist (F. M. Vincentelli et al. 2022). For a sample of 22 quasars, Z. Yu et al. (2020) claimed minimal contamination from the diffuse BLR emission on the lags and H. W. Sharp et al. (2024) suggested a lack of evidence for contributions of the diffuse BLR emission to the lags in 95 luminous quasars.

Here, in Figure 2 we show that the *u*-band excess is a distinguishable prediction for the thermal fluctuation model and reprocessing model with DCE. In the left-hand panel of Figure 2, the median/mean lag-wavelength relation implied by the thermal fluctuation model is monotonic, although the *u*-band excess is found in a few simulations. Instead, the *u*-band excess always exists in each simulation based on the reprocessing model with DCE (the right-hand panel of Figure 2). As expected, future long-term photometric surveys on AGNs, especially quasars with little diffuse BLR emission suggested by Z. Yu et al. (2020) and H. W. Sharp et al. (2024), would shed new light on the nature of the *u*-band excess.

3.4. Are there Correlations Between the Lags and Variation Properties?

A potential positive correlation between the lag and variation amplitude has been observed in NGC 4395 (J. W. Montano et al. 2022; I. M. McHardy et al. 2023). To examine this correlation, we display in Figure 4 the relationship between the lag and variation amplitude implied by both the thermal fluctuation model and reprocessing model with DCE. Interestingly, a positive correlation is predicted by the thermal fluctuation scenario, while the reprocessing model with DCE does not predict such a correlation.

For the reprocessing model with DCE, we find that assuming different variation amplitudes for the driving LC results in more or less the same values of the mean/median lag and scatter in the lags. This explains why the reprocessing model with DCE does not predict a correlation between the interband lag and the variation amplitude. Instead, we find that for the reprocessing model with DCE the lags highly depend on the damping timescale of the driving LC, i.e., a shorter damping timescale generally leads to a smaller interband lag. A similar result has been reported by investigating the lags between the broad emission line and the ionizing UV continuum (M. R. Goad & K. T. Korista 2014, see their Figure 9). Therefore, future measurements on the correlations between the lags and variation properties (e.g., timescale and amplitude) would be useful in distinguishing models for AGN variability.

3.5. How to Infer Model Parameters from the Varied Lags?

If the lags do indeed vary, then averaging the lags measured in repeated and nonoverlapping baselines would be necessary before inferring the model parameters. Adopting the thermal fluctuation scenario, we present how the sparse sampling ($\mathcal{C} = 1$) and the moderate photometric uncertainty ($\mathrm{SNR}_\sigma \simeq 3$) would add scatter to the intrinsic dispersion of the lags. Then, we discuss to what extent the lag-wavelength relation can be accurately measured by considering cases of various sampling cadences ($\mathcal{C} = 3$ or 5) and photometric uncertainties ($\mathrm{SNR}_\sigma \simeq 1$ or 9).

In Figure 5, the colored right-hand portion and gray left-hand portion of the violin plot represent distributions of 200 mock and ideal lags inferred from the mock and ideal LCs, respectively. By comparing dispersions of the ideal lags (the left-hand panel of Figure 2 or $\sigma_{\mathrm{ideal}}/\mu_{\mathrm{ideal}}$) and the mock lags (Figure 5 or $\sigma_{\mathrm{obs}}/\mu_{\mathrm{ideal}}$), the dispersion of the lags is larger, as expected once considering sparse sampling and photometric uncertainty. However, the median values of the mock and ideal lags are comparable (Figure 5). This implies that averaging the lag-wavelength relations of hundreds of AGNs with comparable physical properties could be an efficient way of obtaining the true lag-wavelength relation.

To assess to what extent the true lag-wavelength relation can be accurately measured after averaging the lag-wavelength relations of some AGNs with comparable physical properties, we illustrate in Figure 6 the accuracy quantified by $\langle\sigma_{\mathrm{bs}}(N)/\mu_{\mathrm{ideal}}\rangle_{uriz}$ as a function of the used AGN number, N. On the basis of the lag-wavelength relations of 200 N5548-like AGNs, we average N of them (randomly selected with replacements) for a mean lag-wavelength relation and repeat the selection plus average for 1000 mean lag-wavelength relations whose 1σ dispersion is nominated as $\sigma_{\mathrm{bs}}(N)$. Finally, averaging the ratios of $\sigma_{\mathrm{bs}}(N)$ to μ_{ideal} over *uriz* bands, i.e., $\langle\sigma_{\mathrm{bs}}(N)/\mu_{\mathrm{ideal}}\rangle_{uriz}$, represents the global accuracy achievable by averaging the lag-wavelength relations of N AGNs. Averaging the lag-wavelength relations of $N \sim 20$ AGNs only, an accuracy as high as ∼50% can be easily achieved, but the accuracy increases mildly with further increasing the AGN number, e.g., reaching ∼20% for $N \sim 100$. Instead, increasing finer sampling cadence ($\mathcal{C} \simeq 1$) and/or decreasing photometric uncertainty ($\mathrm{SNR}_\sigma \simeq 9$) are more efficient in obtaining high accuracy for ∼100 AGNs. On the other hand, high accuracy could be achieved even under worse conditions, such as a long sampling cadence ($\mathcal{C} \simeq 5$) and/or low significance of variation ($\mathrm{SNR}_\sigma \simeq 1$), as long as a large number of similar AGNs ($N > 200$) are available.

4. Forecasts for the WFST Survey

To serve as an indispensable complement on the northern sky to the southern LSST surveys, the WFST, located on the summit of Saishiteng Mountain near Lenghu in northwestern China, started the engineering commissioning observations in mid-August 2023. The Deep High-cadence *u*-band Survey (DHS), one of the key programs planned for the WFST 6 yr survey (T. Wang et al. 2023), would cover $\sim 720\,\mathrm{deg}^2$ surrounding the equator and blanketing part of the SDSS Stripe 82 region. Two separate DHS fields of $\sim 360\,\mathrm{deg}^2$ will be continuously monitored for 6 months per year in *ugri* bands and daily cadence (except *u* around the full moon and *i* around the new moon). In addition, both the whole COSMOS field and an area of $\sim 10\,\mathrm{deg}^2$ surrounding the North Ecliptic Pole (NEP) would be monitored in *ugri* bands every night and last for 6 months per year and $\gtrsim 9$ months per year, respectively. Therefore, these WFST surveys are valuable for studying the interband lags of AGNs and examining our prediction of lag

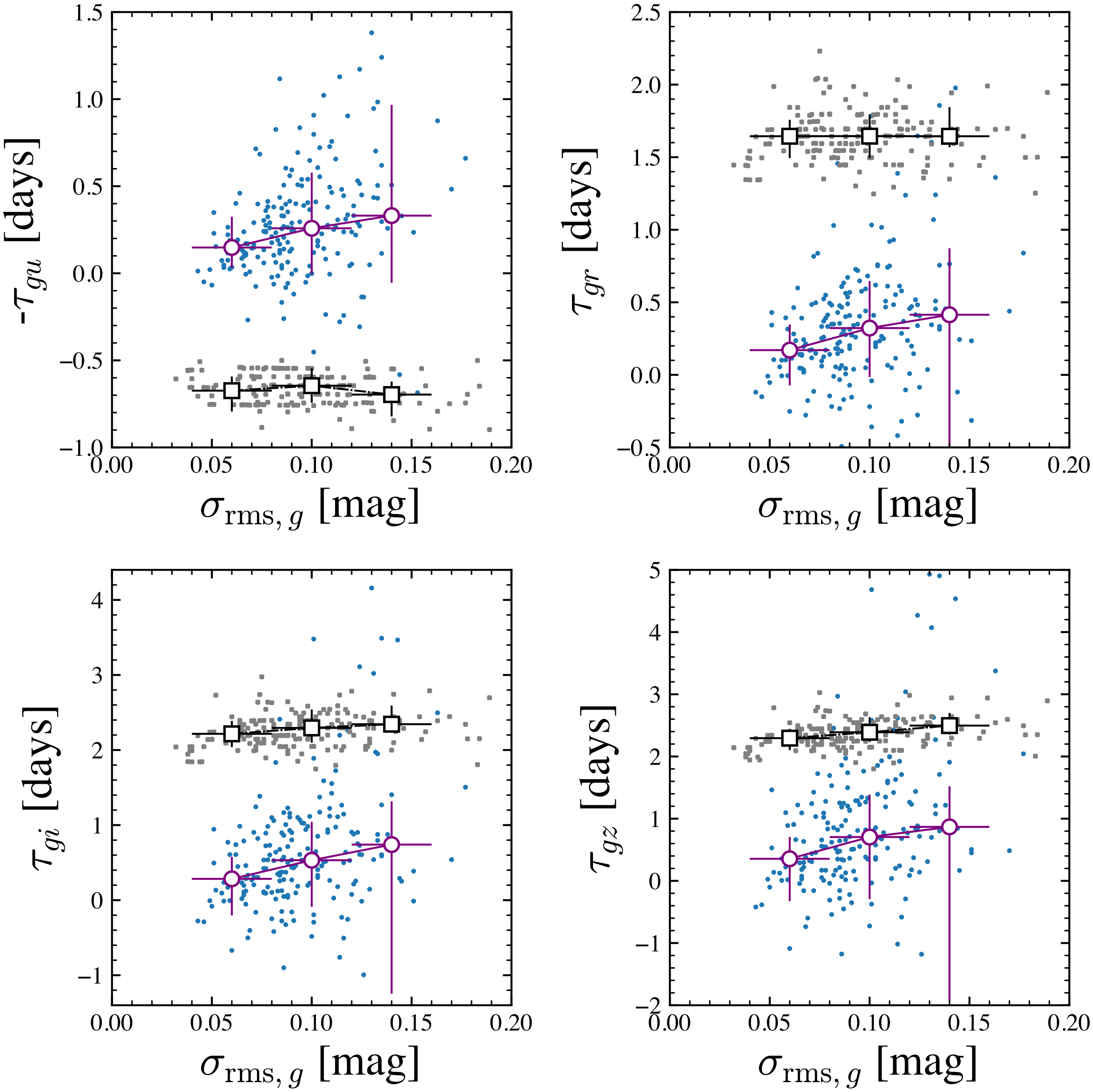

Figure 4. Correlations between the lag of the x band relative to the g band, τ_{gx}, and the g-band variation amplitude, $\sigma_{\mathrm{rms},g}$, where x takes u (top left-hand panel), r (top right-hand panel), i (bottom left-hand panel), and z (bottom right-hand panel), respectively. Values of τ_{gx} and $\sigma_{\mathrm{rms},g}$ from individual simulations are depicted by the small solid symbols, while the corresponding median lag and 16%–84% percentile ranges are shown as the large open symbols with vertical bars in even bins of 0.04 mag. Only bins containing more than 10 data points are shown. Circles are for the thermal fluctuation model, while squares are for the reprocessing model with DCE. The thermal fluctuation model predicts a clear positive correlation between the variation amplitude and the lag (i.e., the larger the variation amplitude, the longer the lag), while the reprocessing model with DCE does not predict such a correlation.

randomness. To suggest an optimal strategy for the interband lag of AGNs with the upcoming formal WFST survey, we perform a series of simulations to assess the effects of diverse observational conditions on the lag measurement based on the thermal fluctuation model, including band selection (e.g., *ugri* or *gri*), sampling cadence (e.g., 2 visits per night or 1 visit per several nights), the variation significance ($\mathrm{SNR}_\sigma \simeq 1$, 3, or 9), duration ($\mathcal{M} = 3$, 6, or 9), and baseline ($\mathcal{Y} = 1$, 2, or 6).

In this section, to quantify the global performance on retrieving the interband lags involving several (at least two) bands and to compare results implied by different observational conditions, we fit the commonly used function form, i.e., $\tau = \tau_g[(\lambda/\lambda_g)^\beta - 1]$ with a fixed β of $4/3$ predicted by the SSD model (e.g., M. M. Fausnaugh et al. 2016; D. Mudd et al. 2018), to our mock lag-wavelength relations, which are measured relative to the g band with an effective wavelength of λ_g, and derive the g-band lags, τ_g, which are assumed to be relative to the X-ray emission of corona located at $\tau = 0$. A positive (negative) τ_g indicates that the X-ray variation leads (lags) the g-band variation. On the one hand, using the CRM method to estimate the disk size, the absolute size of the disk at λ_g is simply taken to be $c\tau_g$, where c is the speed of light. For a negative τ_g, it would result in a weird negative disk size and is generally discarded. For example, H. Guo et al. (2022) got rid of negative lags (<20% in their initial sample) inferred from the CCF analysis between the ZTF g- and r-band LCs. However, negative lags are indeed predicted by the thermal fluctuation scenario (see Figure 2 for ideal simulations). Thus,

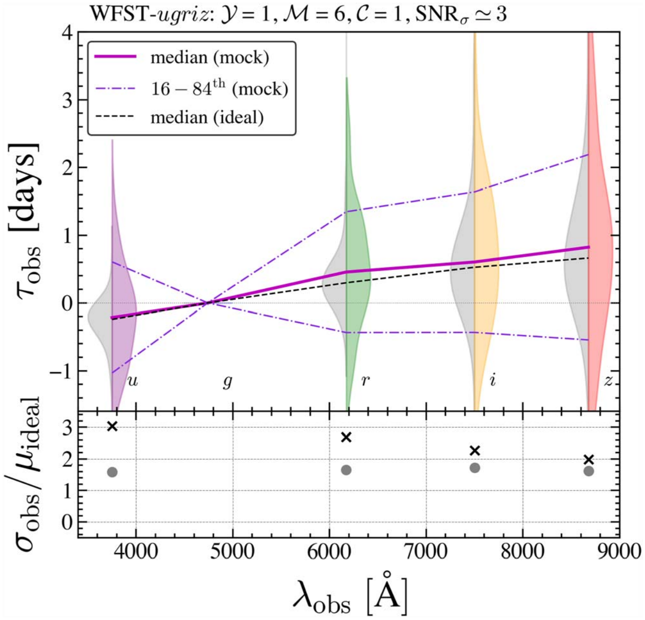

Figure 5. Illustration on how sparse sampling and photometric uncertainty would add scatter to the intrinsic dispersion of the lag in terms of the thermal fluctuation model. In each band, the left-hand portion of the violin plot displays the distribution of 200 ideal lags inferred from the ideal LCs with a very fine cadence and without photometric uncertainty (Figure 2), while the right-hand portion shows that of 200 mock lags inferred from the mock LCs with sparse sampling ($\mathcal{C}=1$) and moderate photometric uncertainty ($\mathrm{SNR}_\sigma \simeq 3$). The median (thick solid line) and 16%–84% percentile ranges (thin dotted–dashed lines) of the mocked lags are compared to the median (thin dashed line) of the ideal lags. This comparison suggests that the median lag-wavelength relations inferred from the mock and ideal LCs are comparable, regardless of the sparse sampling and photometric uncertainty, both of which indeed increase the dispersion of the lag. Dispersion of the mock lags (crosses) and ideal lags (circles) are compared in the lower panel.

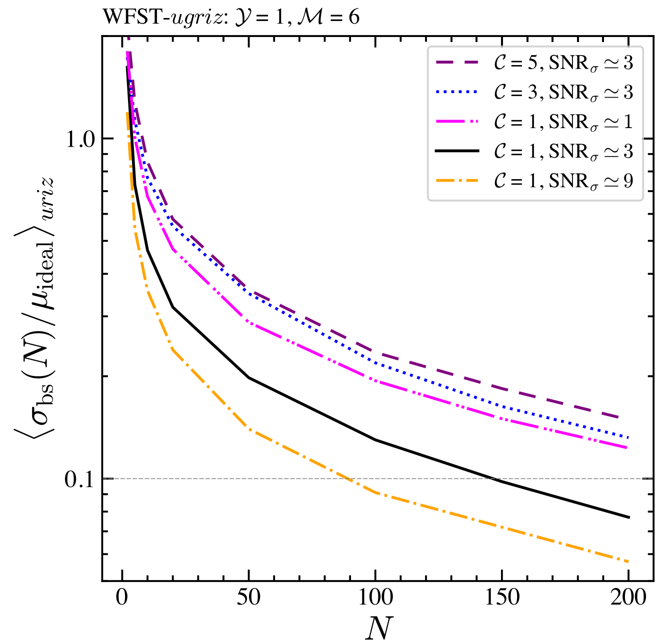

Figure 6. For the thermal fluctuation model, the accuracy of the true lag-wavelength relation obtained by averaging the observed lag-wavelength relations of N AGNs with comparable physical properties for different sampling cadences ($\mathcal{C} \simeq 1$, 3, 5) and photometric uncertainties ($\mathrm{SNR}_\sigma \simeq 1$, 3, 9).

we decide to keep the negative lags inferred from our mock simulations and directly use τ_g for statistics rather than the disk size, $c\tau_g$. On the other hand, as we discussed in Section 2, the foundation of the CRM method may be questionable. Here, the derived τ_g is solely adopted as a common proxy to quantify the effects of diverse observational conditions.

4.1. Observational Effects on the Lag Measurement

4.1.1. Passbands

To analyze the interband lag, it is undeniable that conducting quasi-simultaneous observations in more passbands is a better option, but this requires a large amount of observational times. Panel (a) of Figure 7 illustrates the impact of considering different combinations of WFST bands, i.e., *gr*, *ugr*, *gri*, *ugri*, *griz* and *ugriz*, on the accuracy of measuring τ_g. As the number of bands increases, the dispersion of measured τ_g decreases. However, the decreasing rate of the dispersion becomes quite slow once there are three or more bands involving *gr*. Furthermore, due to the larger time lag τ_{gi} compared to τ_{gu}, the combination of *gri* is expected to have a smaller dispersion compared to *ugr*. We note there are slightly systematic offsets in cases of using *gr* and *ugr* bands, implying that a combination of too few passbands (e.g., *gr*) or too narrow wavelength coverage (e.g., *ugr*) could result in a larger τ_g. Therefore, involving the longer wavelength, e.g., the *i* band, is important in constraining τ_g. In short, we demonstrate that quasi-simultaneous observations in the *gri* bands are preferred. Instead, the combination of *ugri* is also appealing and involving the *u* band can also reveal whether the diffuse continuum emission from the BLR can contaminate that of the accretion disk (e.g., E. M. Cackett et al. 2018; J. W. Montano et al. 2022; H. Netzer 2022) or not (e.g., F. M. Vincentelli et al. 2022; H. W. Sharp et al. 2024).

4.1.2. Sampling Cadence and Variation Significance

In panel (b) of Figure 7, a cadence of approximately 3–5 days leads to a large dispersion in τ_g, while a cadence more frequent than 1 day (i.e., 2 visits per night) does not significantly reduce the dispersion but instead requires double observational times. Therefore, a cadence of 1 day is optimal for the local N5548-like AGNs, as well as high-redshift AGNs thanks to the cosmic time dilation.

In panel (c) of Figure 7, it is clear that increasing SNR_σ from 1 to 9 indeed reduces the dispersion in τ_g. However, the dispersion does not reduce much when SNR_σ increases from 3 to 9. This is because when the photometric uncertainty is very small, the dispersion in τ_g is intrinsic and dominated by the randomness of the lags, predicted by the thermal fluctuation scenario (Section 3). Interestingly, even for $\mathrm{SNR}_\sigma = 1$, the corresponding median lag does not differ much from that implied by $\mathrm{SNR}_\sigma = 9$. This means that even for AGNs with smaller variation amplitude or larger photometric uncertainty, we may still reveal the true interband lag once averaging a large sample of AGNs with similar physical properties.

4.1.3. Duration and Baseline

In panels (d) and (e) of Figure 7, we show the impacts of duration and baseline on the lag measurements, respectively. A slight increase in τ_g with increasing either the duration (within one year) or the baseline (with a fixed duration of 6 months per year) is observed.

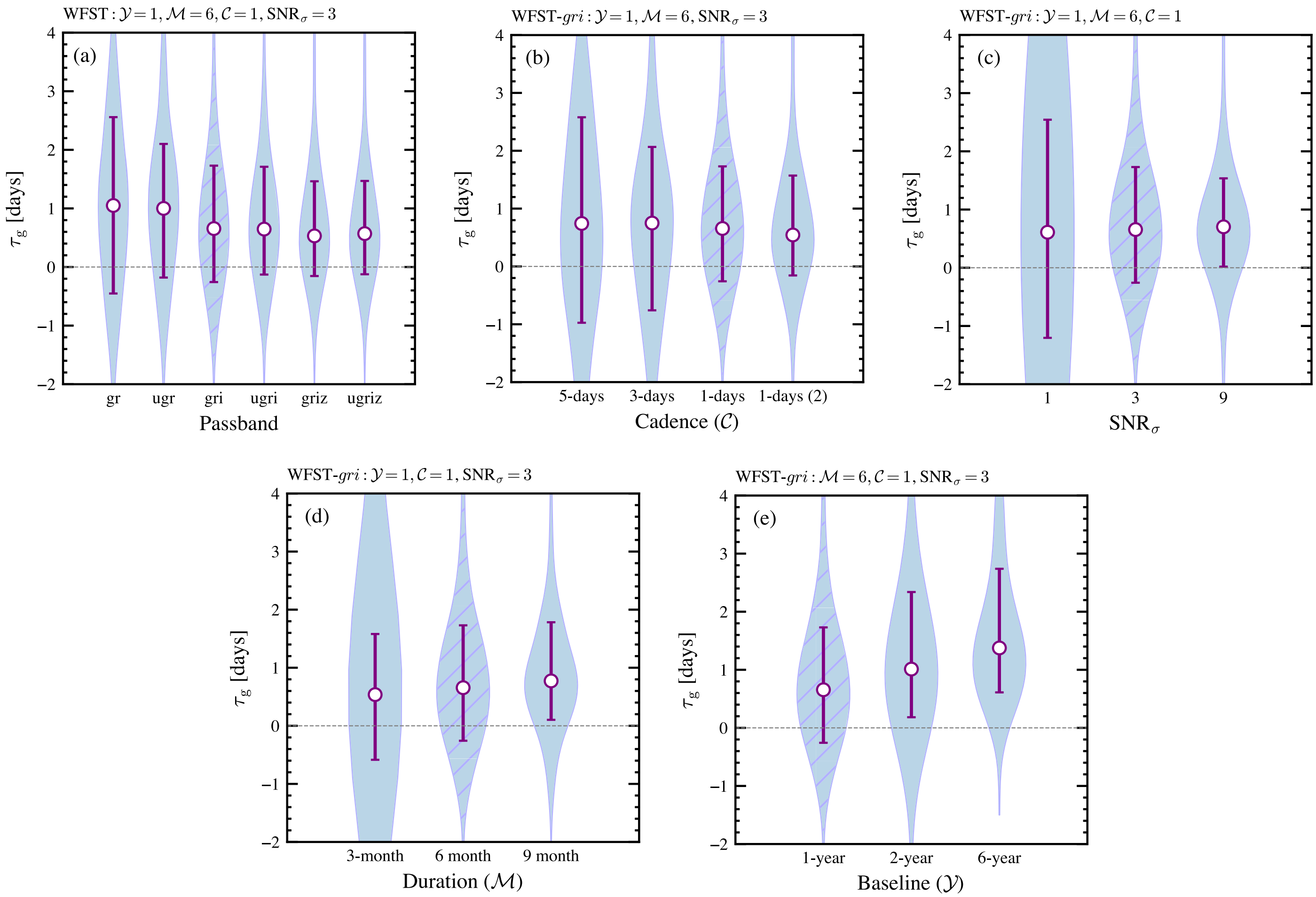

Figure 7. Effects of diverse observational conditions on the lag measurement in terms of the thermal fluctuation model. For each case, the τ_g distribution is shown as a violin plot, overlaid by the median (open circle) and 16%–84% percentile ranges (the vertical bar). The hatched violin plot in each panel refers to the reference case for a combination of {WFST-*gri*, $\mathcal{C} = 1$, SNR$_\sigma = 3$, $\mathcal{M} = 6$, $\mathcal{Y} = 1$}. Each panel illustrates the effect of solely changing one of the conditions compared to the reference case: (a) passband, (b) cadence, (c) variation significance, (d) duration, and (e) baseline.

To explore the dependence of the lag-wavelength relation on both duration ($\mathcal{M} = 3$, 6, 9, and 12) and baseline ($\mathcal{Y} = 1$, 2, 6, and 10) in depth, we illustrate in Figure 8 the median lag-wavelength relations of 200 ideal lag-wavelength relations implied by both the thermal fluctuation model (top panels) and the reprocessing model with DCE (bottom panels). Both models predict a steepening effect for the lag-wavelength relation with increasing duration and baseline. The lag-wavelength relation eventually gets saturation for a sufficiently long baseline. For the reprocessing model with DCE, the saturated lags are found to be consistent with the lags implied by weighting the transfer function adopted. Note that a similar result has been reported by investigating the lags between the broad emission line and the continuum (W. F. Welsh 1999, see Figure 8 therein).

In fact, the measured variation timescale of a LC is biasedly small for a short duration or baseline. Assuming the DRW process, it has been suggested that the LC length should be at least 10 times the damping timescale such that the unbiased variation timescale can be retrieved (e.g., S. Kozłowski 2021; X.-F. Hu et al. 2024). In the reprocessing model with DCE, we adopt $\sim$95 days for the input damping timescale, thus it would require a LC length of at least $\sim$3 yr to retrieve the unbiased variation timescale. Interestingly, according to the bottom panels of Figure 8, the interband lags get saturation for a sufficiently long baseline (i.e., several years), comparable to that required to retrieve the unbiased variation timescale. With the help of upcoming high-cadence and long-term WFST/LSST surveys, investigating the steepening effect of the lag-wavelength relation (Figure 8) as well as the relationship between the interband lag and variation timescale (see also Section 3.4) would shed new light on the underlying physics of AGN variability.

4.2. The Number of Available Local N5548-like AGNs

In this work, we focus on the N5548-like AGNs and suggest that by taking ensemble average over many such AGNs one can derive a reliable underlying lag-wavelength relation. To reach a precision of $\sim$10% for the lag-wavelength relation, we would need a few hundred N5548-like AGNs (Figure 6). Here, we show that these N5548-like AGNs are typical in the local Universe ($z < 0.35$) and there are a few hundred to be covered by the WFST surveys.

The SDSS survey, mainly covering the northern sky, has spectroscopically confirmed $\gtrsim$750, 000 quasars according to its Sixteenth Data Release quasar (DR16Q) catalog (B. W. Lyke et al. 2020). Figure 9 presents the distribution of the r-band magnitude for the DR16Q quasars (dotted histogram) overlapped by the SDSS spectroscopic complete limit (vertical dotted line), as well as the SDSS r-band 5σ detection limit

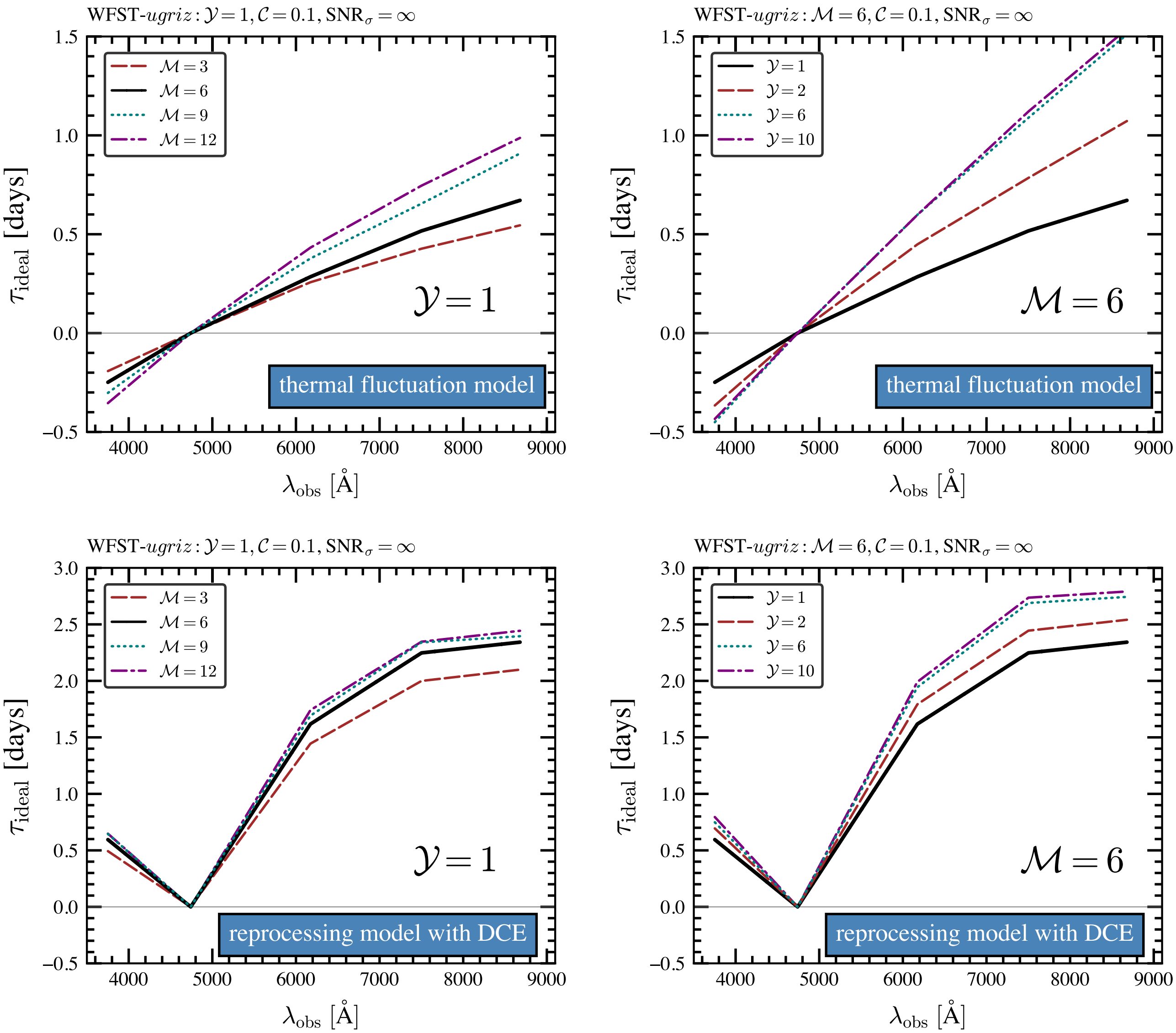

Figure 8. Top panels: Taking the median of 200 ideal lag-wavelength relations inferred from the mock WFST-*ugriz* LCs generated by the thermal fluctuation scenario, the median lag-wavelength relation steepens with increasing duration ($\mathcal{M}$ from 3 months, through 6 and 9, to 12 months in one year; top left-hand panel) and baseline ($\mathcal{Y}$ from 1 yr, through 2 and 6, to 10 yr with a fixed 6 months duration per year; top right-hand panel). Bottom panels: Same as the top panels, but for the prediction of the reprocessing model with DCE.

(vertical dotted–dashed line). In a 90 s exposure, the WFST DHS is expected to reach a 5σ detection limit in the r band ($\sim$23.7 mag, vertical dashed line; L. Lei et al. 2023)[14] deeper than that of the SDSS. Although the WFST surveys would provide valuable long-term variation data (weekly cadence in the WFST wide-field survey) for a majority of the SDSS DR16Q quasars, only a portion of them located within the WFST DHS and at relatively low redshift are suitable for analyzing the interband lag.

H.-Y. Liu et al. (2019) constructed a uniform, complete sample of broad-line AGNs in the local Universe ($z < 0.35$) selected from the SDSS Seventh Data Release quasar (DR7Q) catalog. The corresponding distribution of the r-band magnitude is shown as the solid histogram in the left-hand panel of Figure 9. Additionally, the right-hand panel of Figure 9 shows the density map in $\log \lambda_{\rm Edd}$ versus $\log M_{\rm BH}$ by scaling the density map of the H.-Y. Liu et al. (2019) sample in 9376–1000 deg^2. These local AGNs have typical $\log(M_{\rm BH}/M_\odot) \simeq 7.6$ and $\log \lambda_{\rm Edd} \simeq -1.3$ (i.e., the star in the right-hand panel of Figure 9), indeed similar to NGC 5548. The number of available N5548-like AGNs to be covered by the WFST DHS is several hundred (and more if selecting similar AGNs from the SDSS DR16Q). Therefore, we expect that there are enough N5548-like AGNs in the WFST DHS valuable to analyze the interband lag of AGN.

4.3. WFST versus Other Time Domain Surveys

In addition to WFST, there are many ongoing and upcoming time domain surveys, such as PS1, ZTF, and LSST. Exploring the interband variation properties of AGNs is usually itemized as one of their scientific goals. Table 1 presents the general information of these surveys compared to the WFST DHS. Figure 10 illustrates the resultant performance of these surveys

[14] The WFST r-band 5σ detection limit in a 90 s exposure is calculated for conditions of airmass = 1.20, seeing = 0$''$.75 at the darkest New Moon night of the Lenghu site ($V = 22.30$ mag, Moon phase $\theta = 0°$). The code for the detection limit is available at https://github.com/Leilei-astro/WFST-limiting-magnitudes.

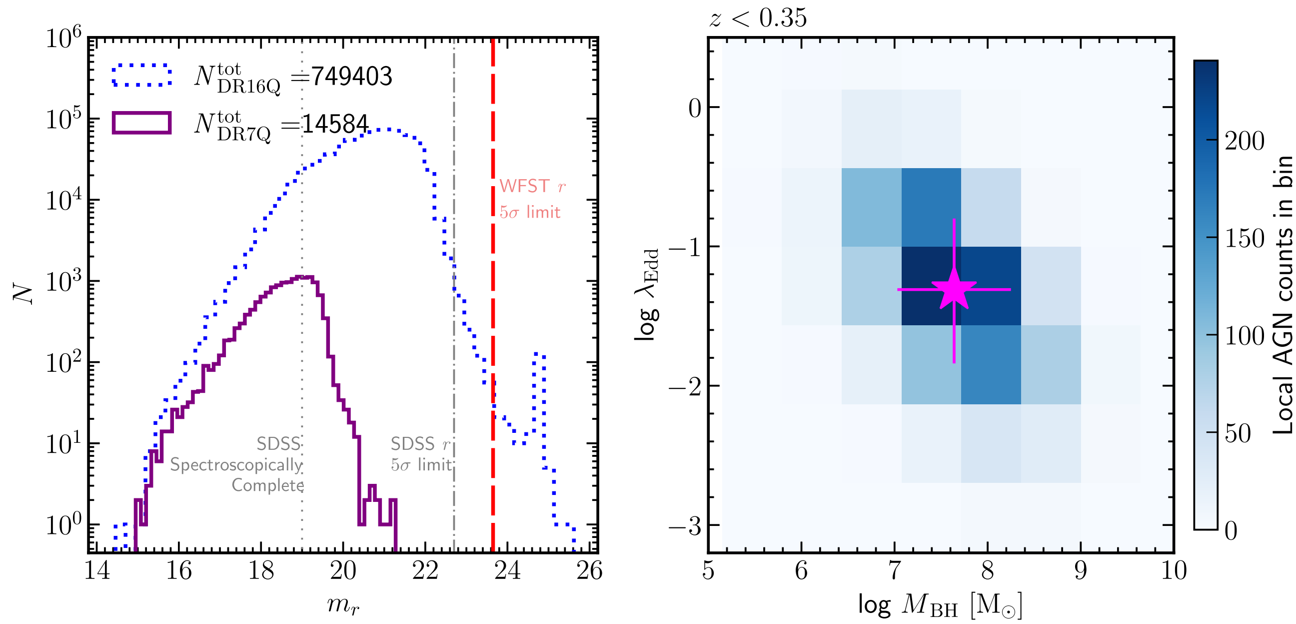

Figure 9. Left-hand panel: Distributions of the apparent r-band magnitudes for spectroscopically confirmed quasars in the SDSS DR16Q catalog (dotted histogram; B. W. Lyke et al. 2020) and a uniform, complete sample of broad-line AGNs at $z < 0.35$ selected from the SDSS DR7Q catalog (solid histogram; H.-Y. Liu et al. 2019). Note that only quasars with physical r-band magnitudes are used here. Shown for comparison are the spectroscopically complete limit of $\sim$19 mag for the SDSS quasars (vertical dotted line) and the WFST r-band 5σ detection limit of $\sim$23.7 mag in a single 90 s exposure (vertical dashed line; L. Lei et al. 2023), which is deeper than that of the SDSS-r band (vertical dotted–dashed line). Right-hand panel: The density map in $\log M_{\rm BH}$ vs. $\log \lambda_{\rm Edd}$ for local N5548-like AGNs expected in $\sim$1000 deg^2, to be monitored by the WFST DHS, by scaling that of the H.-Y. Liu et al. (2019) sample covering 9376 deg^2. The star and horizontal (or vertical) bar indicate the median and 16%–84% percentile ranges of $\log M_{\rm BH}$ (or $\log \lambda_{\rm Edd}$) of the H.-Y. Liu et al. (2019) sample.

Table 1
Information of Four Main Time Domain Surveys

Survey	Filter	r-band 5σ Detection Limit (mag)	Cadence (day)	Coverage (deg^2)	SNR$_\sigma$ [a]	Advantages of WFST[b]
LSST DDF[c]	*ugriz*	24.7	2	40	9	I, II
WFST DHS	(u)gri(z)	23.7	1	720	3	I. finer cadence,
…	…	…	…	…	…	II. larger sky region,
…	…	…	…	…	…	III. deeper in detection limit,
…	…	…	…	…	…	IV. more quasi-simultaneous bands.
PS1 MDS[d]	gr(iz)	23.3	3	70	3	I, II, III, IV
ZTF 3π[e]	gr(i)	20.6	3	$\sim$30,000	3	I, III, IV

Notes.
[a] The SNR$_\sigma$ equals $\langle\sigma_{\rm rms}\rangle/\sigma_{\rm e}$, where $\langle\sigma_{\rm rms}\rangle$ we simulate is 0.083 mag in the case of $\mathcal{Y} = 1$ and $\mathcal{M} = 6$. A typical $\sigma_{\rm e}$ of $\simeq$0.03 mag (or SNR$_\sigma \simeq 3$) is adopted for ZTF (e.g., H. Guo et al. 2022; W.-J. Guo et al. 2022; V. K. Jha et al. 2022), PS1 (K. L. Suberlak et al. 2021), and WFST, while 3 times better is assumed for LSST.
[b] Four potential advantages of the WFST DHS are nominated and the corresponding points are itemized when compared with the relevant surveys.
[c] The survey strategy of the LSST DDF has not yet been settled. Hence, we adopt that proposed by W. N. Brandt et al. (2018): four visits in u, one visit in g, one visit in r, three visits in i, five visits in z for every two nights. The r-band 5σ detection limit and the coverage of the LSST DDF are also taken from W. N. Brandt et al. (2018).
[d] According to K. C. Chambers et al. (2016), the Medium Deep Survey (MDS) of the PS1 repeats monitoring *griz* bands in a 3 days cycle: *gr* in the first night, r in the second, and z in the third. The r-band 5σ detection limit and the coverage of the PS1 MDS are also taken from K. C. Chambers et al. (2016).
[e] ZTF maps a 3π sky at cadences of $\sim$3 days in *gr* bands mainly (M. J. Graham et al. 2019). The r-band 5σ detection limit is taken from F. J. Masci et al. (2019).

on the lag measurement, adopting the same $\mathcal{Y} = 1$ and $\mathcal{M} = 6$ for N5548-like AGNs.

Compared to ZTF, WFST has a better performance on the lag measurement thanks to its advantage of quasi-simultaneous observations in the *gri* bands with a finer cadence of approximately 1 day.

The performances of PS1 and WFST are comparable. Although PS1 has a sparser cadence than WFST, the inclusion of the PS1 z band indeed helps improve the quality of the lag measurement. Instead, the WFST DHS has a $\simeq$10 times larger sky coverage, and thus could give rise to a higher accuracy on the lag measurement once ensemble averaging the lag-wavelength relations of a larger sample of AGNs.

The performance of the LSST DDF is appealing. Nevertheless, the WFST DHS, with a daily cadence in *gri* bands and a large sky coverage, makes it a competitive survey for exploring the interband lag of AGNs.

5. Conclusions

In this work, we analyze the random behavior of the lag-wavelength relations based on two models for AGN variability, i.e., the thermal fluctuation model and the reprocessing model

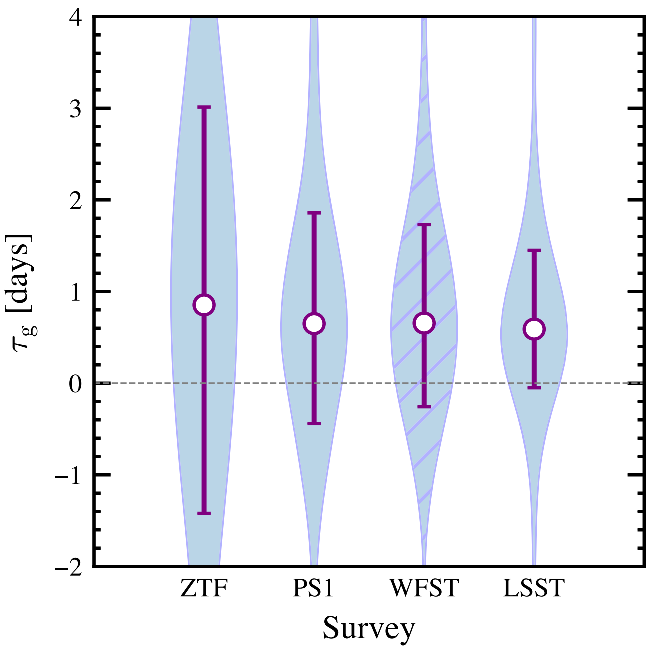

Figure 10. Same as Figure 7 but comparing the performance of different survey strategies of the ongoing and upcoming time domain surveys (see Table 1), adopting the same $\mathcal{Y} = 1$ and $\mathcal{M} = 6$.

with DCE. Our simulations reveal that for both models the measured lags can differ from one finite duration/baseline to another, owing to the random nature of AGN variability.

Given a finite duration/baseline, the thermal fluctuation model predicts a larger scatter in the lags, more violent lag evolution, and fewer cases of the u-band excess than the reprocessing model with DCE. In addition, a positive correlation between the interband lag and the variation amplitude is expected by the thermal fluctuation scenario, but not the reprocessing model with DCE. Future long-term, high-cadence monitoring on a sample of AGNs will be essential to test these predictions and refine models.

We suggest that for both models averaging the lags measured in repeated and nonoverlapping baselines can achieve a stable lag. The longer the duration/baseline, the larger the averaged lag. The averaged lag would get saturation for a sufficiently long LC. Obtaining the average lag for an individual AGN requiring a sufficiently long LC is observationally challenging. Instead, averaging the lags of a sample of AGNs with similar physical properties is achievable and can be equivalently used to constrain the model parameters.

Finally, we perform a series of simulations to assess the observational effects of diverse conditions on the lag measurement based on the thermal fluctuation model. We suggest an optimal strategy, i.e., a daily cadence in gri bands with 6 months of continuous monitoring per year, to study the interband lag of AGN variability with the upcoming formal WFST DHS. The resultant WFST measurements on the interband lags are expected to be better than ZTF/PS1 and competitive with LSST.

Acknowledgments

We are grateful to the anonymous referee for the many constructive suggestions which have significantly improved our manuscript, and we thank X. Kong for the helpful comments. This work is supported by the National Key R&D Program of China (grant No. 2023YFA1608100) and the National Science Foundation of China (grant Nos. 12373016, 12033006, 12025303, 12173037, and 12233008). Z.Y.C. is supported by the science research grants from the China Manned Space Project under grant no. CMS-CSST-2021-A06 and the Cyrus Chun Ying Tang Foundations. L.L.F. acknowledges the CAS Project for Young Scientists in Basic Research (No. YSBR-092) and the Fundamental Research Funds for the Central Universities (WK3440000006). Z.Z.H. acknowledges the National Postdoctoral Grant Program (No GZC20232990). Z.C.H. is supported by the National Natural Science Foundation of China (Nos. 12222304, 12192220, and 12192221). G.L.L acknowledges the support from the China Manned Space Project (the second-stage CSST science project: "Investigation of small-scale structures in galaxies and forecasting of observations") and the National Natural Science Foundation of China (No. 12273036).

ORCID iDs

Zhen-Bo Su https://orcid.org/0000-0001-8515-7338
Zhen-Yi Cai https://orcid.org/0000-0002-4223-2198
Jun-Xian Wang https://orcid.org/0000-0002-4419-6434
Tinggui Wang https://orcid.org/0000-0002-1517-6792
Yongquan Xue https://orcid.org/0000-0002-1935-8104
Min-Xuan Cai https://orcid.org/0000-0003-4721-6477
Lulu Fan https://orcid.org/0000-0003-4200-4432
Hengxiao Guo https://orcid.org/0000-0001-8416-7059
Zhicheng He https://orcid.org/0000-0003-3667-1060
Zizhao He https://orcid.org/0000-0001-8554-9163
Xu-Fan Hu https://orcid.org/0009-0006-9884-6128
Ji-an Jiang https://orcid.org/0000-0002-9092-0593
Ning Jiang https://orcid.org/0000-0002-7152-3621
Wen-Yong Kang https://orcid.org/0000-0003-2573-8100
Lei Lei https://orcid.org/0000-0003-4631-1915
Guilin Liu https://orcid.org/0000-0003-2390-7927
Teng Liu https://orcid.org/0000-0002-2941-6734
Zhengyan Liu https://orcid.org/0000-0002-2242-1514
Zhenfeng Sheng https://orcid.org/0000-0001-6938-8670
Mouyuan Sun https://orcid.org/0000-0002-0771-2153
Wen Zhao https://orcid.org/0000-0002-1330-2329

References

Abbott, T. M. C., Abdalla, F. B., Allam, S., et al. 2018, ApJS, 239, 18
Antonucci, R. 2013, Natur, 495, 165
Antonucci, R. 2015, arXiv:1501.02001
Antonucci, R. 2018, NatAs, 2, 504
Antonucci, R. R. J. 2023, Galax, 11, 102
Bate, N. F., Vernardos, G., O'Dowd, M. J., et al. 2018, MNRAS, 479, 4796
Brandt, W. N., Ni, Q., Yang, G., et al. 2018, arXiv:1811.06542
Cackett, E. M., Bentz, M. C., & Kara, E. 2021, iSci, 24, 102557
Cackett, E. M., Chiang, C.-Y., McHardy, I., et al. 2018, ApJ, 857, 53
Cackett, E. M., & Horne, K. 2006, MNRAS, 365, 1180
Cackett, E. M., Zoghbi, A., & Ulrich, O. 2022, ApJ, 925, 29
Cai, Z.-Y., & Wang, J.-X. 2023, NatAs, 7, 1506
Cai, Z.-Y., Wang, J.-X., & Sun, M. 2020, ApJ, 892, 63
Cai, Z.-Y., Wang, J.-X., Zhu, F.-F., et al. 2018, ApJ, 855, 117
Chambers, K. C., Magnier, E. A., Metcalfe, N., et al. 2016, arXiv:1612.05560
Chan, J. H. H., Millon, M., Bonvin, V., & Courbin, F. 2020, A&A, 636, A52
Chelouche, D., Pozo Nuñez, F., & Kaspi, S. 2019, NatAs, 3, 251
Cho, H., Woo, J.-H., Treu, T., et al. 2021, ApJ, 921, 98
Cornachione, M. A., & Morgan, C. W. 2020, ApJ, 895, 93
Dai, X., Kochanek, C. S., Chartas, G., et al. 2010, ApJ, 709, 278
De Rosa, G., Peterson, B. M., Ely, J., et al. 2015, ApJ, 806, 128
Dexter, J., & Agol, E. 2011, ApJL, 727, L24
Edelson, R., Gelbord, J., Cackett, E., et al. 2017, ApJ, 840, 41

Edelson, R., Gelbord, J., Cackett, E., et al. 2019, ApJ, 870, 123
Edelson, R., Peterson, B. M., Gelbord, J., et al. 2024, ApJ, 973, 152
Edelson, R. A., & Krolik, J. H. 1988, ApJ, 333, 646
Fausnaugh, M. M., Denney, K. D., Barth, A. J., et al. 2016, ApJ, 821, 56
Fausnaugh, M. M., Starkey, D. A., Horne, K., et al. 2018, ApJ, 854, 107
Gallo, L. C., Blue, D. M., Grupe, D., Komossa, S., & Wilkins, D. R. 2018, MNRAS, 478, 2557
Gardner, E., & Done, C. 2017, MNRAS, 470, 3591
Gaskell, C. M. 2006, in ASP Conf. Ser. 360, AGN Variability from X-Rays to Radio Waves, ed. C. M. Gaskell et al. (San Francisco, CA: ASP), 111
Gaskell, C. M. 2017, MNRAS, 467, 226
Gaskell, C. M., Klimek, E. S., & Nazarova, L. S. 2007, arXiv:0711.1025
Goad, M. R., & Korista, K. T. 2014, MNRAS, 444, 43
Goad, M. R., Korista, K. T., De Rosa, G., et al. 2016, ApJ, 824, 11
Graham, M. J., Kulkarni, S. R., Bellm, E. C., et al. 2019, PASP, 131, 078001
Guo, H., Barth, A. J., & Wang, S. 2022, ApJ, 940, 20
Guo, W.-J., Li, Y.-R., Zhang, Z.-X., Ho, L. C., & Wang, J.-M. 2022, ApJ, 929, 19
Hagen, S., Done, C., & Edelson, R. 2024, MNRAS, 530, 4850
Hall, P. B., Sarrouh, G. T., & Horne, K. 2018, ApJ, 854, 93
Hernández Santisteban, J. V., Edelson, R., Horne, K., et al. 2020, MNRAS, 498, 5399
Homayouni, Y., Trump, J. R., Grier, C. J., et al. 2019, ApJ, 880, 126
Hu, X.-F., Cai, Z.-Y., & Wang, J.-X. 2024, ApJ, 961, 5
Jaiswal, V. K., Prince, R., Panda, S., & Czerny, B. 2023, A&A, 670, A147
Jha, V. K., Joshi, R., Chand, H., et al. 2022, MNRAS, 511, 3005
Jiang, Y.-F., Green, P. J., Greene, J. E., et al. 2017, Apj, 836, 186
Jiménez-Vicente, J., Mediavilla, E., Kochanek, C. S., et al. 2014, ApJ, 783, 47
Kammoun, E. S., Papadakis, I. E., & Dovčiak, M. 2021, MNRAS, 503, 4163
Kara, E., Barth, A. J., Cackett, E. M., et al. 2023, ApJ, 947, 62
Kokubo, M. 2018, PASJ, 70, 97
Korista, K. T., & Goad, M. R. 2019, MNRAS, 489, 5284
Kovačević, A. B., Ilić, D., Popović, L. Č., et al. 2021, MNRAS, 505, 5012
Kovačević, A. B., Radović, V., Ilić, D., et al. 2022, ApJS, 262, 49
Kozłowski, S. 2021, AcA, 71, 103
Krolik, J. H., Horne, K., Kallman, T. R., et al. 1991, Apj, 371, 541
Lawther, D., Goad, M. R., Korista, K. T., Ulrich, O., & Vestergaard, M. 2018, MNRAS, 481, 533
Lei, L., Zhu, Q.-F., Kong, X., et al. 2023, RAA, 23, 035013
Li, T., Sun, M., Xu, X., et al. 2021, ApJL, 912, L29
Li, Y.-P., Yuan, F., & Dai, X. 2019, MNRAS, 483, 2275
Liu, H.-Y., Liu, W.-J., Dong, X.-B., et al. 2019, ApJS, 243, 21
Lyke, B. W., Higley, A. N., McLane, J. N., et al. 2020, ApJS, 250, 8
Maoz, D., Markowitz, A., Edelson, R., & Nandra, K. 2002, AJ, 124, 1988
Masci, F. J., Laher, R. R., Rusholme, B., et al. 2019, PASP, 131, 018003
McHardy, I. M., Beard, M., Breedt, E., et al. 2023, MNRAS, 519, 3366
Montano, J. W., Guo, H., Barth, A. J., et al. 2022, ApJL, 934, L37
Morales, A. M., Miller, J. M., Cackett, E. M., Reynolds, M. T., & Zoghbi, A. 2019, ApJ, 870, 54
Moran, E. C., Eracleous, M., Leighly, K. M., et al. 2005, AJ, 129, 2108
Morgan, C. W., Hyer, G. E., Bonvin, V., et al. 2018, ApJ, 869, 106
Mudd, D., Martini, P., Zu, Y., et al. 2018, ApJ, 862, 123
Netzer, H. 2022, MNRAS, 509, 2637
Pal, M., Dewangan, G. C., Connolly, S. D., & Misra, R. 2017, MNRAS, 466, 1777
Peterson, B. M., Wanders, I., Horne, K., et al. 1998, PASP, 110, 660
Pozo Nuñez, F., Bruckmann, C., Deesamutara, S., et al. 2023, MNRAS, 522, 2002
Shakura, N. I., & Sunyaev, R. A. 1973, A&A, 24, 337
Sharp, H. W., Homayouni, Y., Trump, J. R., et al. 2024, ApJ, 961, 93
Shen, Y., Brandt, W. N., Dawson, K. S., et al. 2015, ApJS, 216, 4
Sou, H., Wang, J.-X., Xie, Z.-L., Kang, W.-Y., & Cai, Z.-Y. 2022, MNRAS, 512, 5511
Starkey, D., Horne, K., Fausnaugh, M. M., et al. 2017, ApJ, 835, 65
Starkey, D. A., Huang, J., Horne, K., & Lin, D. N. C. 2023, MNRAS, 519, 2754
Suberlak, K. L., Ivezić, Ž., & MacLeod, C. 2021, ApJ, 907, 96
Sun, M., Grier, C. J., & Peterson, B. M. 2018, PyCCF: Python Cross Correlation Function for Reverberation Mapping Studies, Astrophysics Source Code Library, ascl:1805.032
Sun, M., Xue, Y., Brandt, W. N., et al. 2020, ApJ, 891, 178
Sun, M., Xue, Y., Trump, J. R., & Gu, W.-M. 2019, MNRAS, 482, 2788
Tie, S. S., & Kochanek, C. S. 2018, MNRAS, 473, 80
Vasudevan, R. V., & Fabian, A. C. 2009, MNRAS, 392, 1124
Vaughan, S., Edelson, R., Warwick, R. S., & Uttley, P. 2003, MNRAS, 345, 1271
Vincentelli, F. M., Beard, M., Hardy, I. M., et al. 2023, AN, 344, e20230018
Vincentelli, F. M., McHardy, I., Hernández Santisteban, J. V., et al. 2022, MNRAS, 512, L33
Wang, T., Liu, G., Cai, Z., et al. 2023, SCPMA, 66, 109512
Welsh, W. F. 1999, PASP, 111, 1347
Wilkins, D. R. 2023, MNRAS, 526, 3441
Yu, Z., Martini, P., Davis, T. M., et al. 2020, ApJS, 246, 16
Zhu, F.-F., Wang, J.-X., Cai, Z.-Y., et al. 2018, ApJ, 860, 29
Zoghbi, A., Reynolds, C., & Cackett, E. M. 2013, ApJ, 777, 24